Monthly Notices
of the
ROYAL ASTRONOMICAL SOCIETY

MNRAS **480,** 5084–5091 (2018)
Advance Access publication 2018 August 18

doi:10.1093/mnras/sty2260

Globular clusters versus dark matter haloes in strong lensing observations

Qiuhan He,[1,2] Ran Li,[1,2]★ Sungsoon Lim,[3,4] Carlos S. Frenk,[5] Shaun Cole,[5] Eric W. Peng[3,4] and Qiao Wang[1,2]

[1]*Key Laboratory for Computational Astrophysics, National Astronomical Observatories, Chinese Academy of Sciences, Beijing 100012, China*
[2]*University of Chinese Academy of Sciences, 19 A Yuquan Rd, Shijingshan District, Beijing 100049, China*
[3]*Department of Astronomy, Peking University, Beijing 100871, China*
[4]*Kavli Institute for Astronomy and Astrophysics, Peking University, Beijing 100871, China*
[5]*Institute for Computational Cosmology, Department of Physics, University of Durham, South Road, Durham DH1 3LE, UK*

Accepted 2018 August 14. Received 2018 August 3; in original form 2017 July 6

ABSTRACT

Small distortions in the images of Einstein rings or giant arcs offer the exciting prospect of detecting low mass dark matter haloes or subhaloes of mass below 10^9 $M_\odot$ (for independent haloes, the mass refers to M_{200}, and for subhaloes, the mass refers to the mass within tidal radius), most of which are too small to have made a visible galaxy. A very large number of such haloes are predicted to exist in the cold dark matter model of cosmogony; in contrast, other models, such as warm dark matter, predict no haloes below a mass of this order, which depends on the properties of the warm dark matter particle. Attempting to detect these small perturbers could therefore discriminate between different kinds of dark matter particles, and even rule out the cold dark matter model altogether. Globular clusters in the lens galaxy also induce distortions in the image, which could, in principle, contaminate the test. Here, we investigate the population of globular clusters in six early-type galaxies in the Virgo cluster. We find that the number density of globular clusters of mass $M_{\rm GC} \sim 10^6$ $M_\odot$ is comparable to that of the dark matter perturbers (subhaloes in the lenses and haloes along the line of sight of comparable mass). We show that the very different degrees of mass concentration in globular clusters and dark matter haloes result in different lensing distortions. These are detectable with milli-arcsecond resolution imaging, which can distinguish between globular cluster and dark matter halo signals.

Key words: gravitational lensing: strong – globular clusters: general – dark matter.

1 INTRODUCTION

Perhaps the most fundamental prediction of cosmogonic models in which the dark matter consists of cold collisionless particles (cold dark matter, CDM), such as the current cosmological paradigm, ΛCDM, is the existence of a very large number of dark matter haloes with masses extending well below the masses of even the faintest galaxies known (e.g. down to an Earth mass for a few GeV weakly interacting particle; Green, Hofmann & Schwarz 2005; Diemand, Kuhlen & Madau 2007; Springel et al. 2008; Frenk & White 2012). This property distinguishes CDM models from models in which the dark matter is a warm particle (warm dark matter, WDM) such as sterile neutrino (Boyarsky, Ruchayskiy & Shaposhnikov 2009). In this case, particle free streaming in the early universe induces a low-mass cut-off in the power spectrum of density perturbations. As a result, few dark matter haloes of mass less than about 10^8 $M_\odot$ (depending on the particle properties; see Bose et al. 2016; Lovell et al. 2016) ever form. Searching for haloes smaller than about 10^8 $M_\odot$ provides a clear-cut way to distinguish between these dark matter candidates. Finding a handful of dark matter haloes of mass, say 10^7 $M_\odot$, would rule out most WDM models of interest. Conversely, failing to find such haloes would conclusively rule out CDM models, including ΛCDM.

A major difficulty in applying this test is that the haloes of interest are too small ever to have made a galaxy and are thus completely dark (see Sawala et al. 2016 and references therein). For this reason, attempts to test CDM or distinguish it from WDM using the abundance of the more massive haloes that do make a galaxy are misguided: many studies dating back to semi-analytic models in the early 2000s (Bullock, Kravtsov & Weinberg 2000; Benson et al. 2002; Somerville 2002) and, more recently, using hydrodynamic simulations (e.g. Macciò et al. 2006; Okamoto & Frenk 2009; Sawala et al. 2016; Wetzel et al. 2016) have clearly demonstrated that physically based ΛCDM models predict the correct number of faint galaxies, including satellites of the Milky Way. By contrast,

★ E-mail: ranl@bao.ac.cn

the observed abundance of satellites can be used to rule out regions of the WDM parameter space (Kennedy et al. 2014; Lovell et al. 2016).

A conclusive test of CDM and many other particle dark matter candidates requires counting dark, small-mass haloes. Fortunately, these are detectable through gravitational lensing, specifically through the distortions they induce in strongly lensed systems that produce Einstein rings or giant arcs (Koopmans 2005; Vegetti & Koopmans 2009a,b; Vegetti et al. 2012; Hezaveh et al. 2016; Li et al. 2016). Until recently, it was thought that the distortions would come from substructures inside the lens. However, Li et al. (2017) and Despali et al. (2017) have recently shown that the distortions in CDM and WDM models are dominated by intervening haloes projected onto the Einstein ring or strong lens rather than by subhaloes in the lens. This is a fortunate feature because it makes the test of particle candidates particularly clean: small-mass intervening haloes are not affected in any way by baryon effects, unlike subhaloes some of which can be destroyed by interaction with the central galaxy (Garrison-Kimmel et al. 2017; Sawala et al. 2017).

For the lensing test to be effective, it is essential to be able to detect subhaloes of small mass (Li et al. 2016). The detection limit of a particular observation depends on the resolution of the imaging. Vegetti et al. (2010) detected an object of $3.51 \pm 0.15 \times 10^9$ $M_\odot$ in a strong lens system with *Hubble Space Telescope* (*HST*) imaging. With higher resolution imaging from adoptive optics on the Keck telescope, Vegetti et al. (2012) detected a $1.9 \pm 0.1 \times 10^8$ $M_\odot$ object in a lens galaxy at redshift 0.88; they argued that with data of this quality, objects down to $\sim 10^7$ $M_\odot$ could be detected. Simulations suggest that even smaller haloes, down to 10^6 $M_\odot$,[1] can be detected in radio-selected strong lenses (McKean et al. 2015).

Li et al. (2016) recently investigated the sample size and detection limit required to distinguish ΛCDM from the particularly interesting WDM model in which the particles are 7 keV sterile neutrinos whose decay could explain the 3.5 keV X-ray line recently detected in galaxies and clusters (Boyarsky et al. 2014; Bulbul et al. 2014). In this case, the cut-off in the halo mass function occurs at a mass of $\sim 10^8$ $M_\odot$ (Bose et al. 2016; Li et al. 2016).[2]

To count the number of subhaloes and line-of-sight haloes in a consistent way, Li et al. (2017) defined an effective mass, $M_{\rm eff}$, for dark matter perturbers as the best-fitting value of M_{200} for an NFW halo (Navarro, Frenk & White 1996, 1997) at the lens redshift. Li et al. (2017) showed that, with a detection limit of $M_{\rm eff,\,lim}=10^7$ $M_\odot$, $\sim$20−100 lenses would suffice to distinguish even the coldest 7 kev sterile neutrino model allowed by the X-ray data from CDM. Li et al. (2016) also showed that the constraining power increases rapidly with improvements in the detection limit. If very long baseline interferometry (VLBI) imaging could really reach a detection limit of 10^6 $M_\odot$, a handful of lens systems would already be enough conclusively to rule out all 7 keV sterile neutrinos, if a signal is found, or CDM if it is not.

[1] Vegetti et al. (2010, 2012) fit the structure with a tidally truncated pseudo-Jaffe profile. The mass quoted for McKean et al. (2015) is the mass for an SIS halo truncated at Einstein radius. Despali et al. (2017) have shown that, for a given object, the NFW virial mass is between half and one order of magnitude larger than the pseudo-Jaffe total mass.

[2] For independent haloes, the masses quoted correspond to M_{200}, the mass enclosed within a radius within which the average density equals to 200 times of critical density; for subhaloes, the masses quoted are those assigned by the SUBFIND subhalo finder, which correspond to the mass within the tidal radius (Springel et al. 2008).

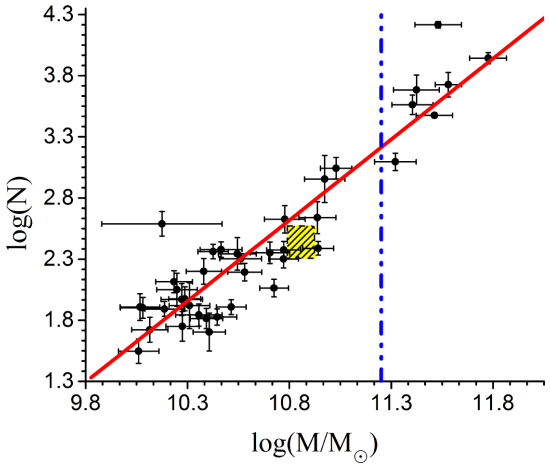

Figure 1. The relation between the number of globular clusters, *N*, and the host galaxy stellar mass. The rectangle marks the location of the Milky Way in this plane. Galaxies to the right of the vertical dashed line have similar masses to the galaxies in the SLACS sample (Bolton et al. 2008).

A potential complication arises because dark matter haloes and subhaloes are not the only objects that can perturb an Einstein ring. Globular clusters in the lens galaxy could also be a source of perturbations. Studies of nearby galaxies show that the mass function of globular clusters has a Gaussian distribution peaking at about 10^5 $M_\odot$ (Jordán et al. 2007). In the Milky Way, the largest globular cluster is ω Centauri, which has a mass of $4.05 \pm 0.1 \times 10^6$ $M_\odot$ (D'Souza & Rix 2013). Since the globular clusters have much more concentrated mass profiles than NFW haloes, they can produce a stronger signal than dark matter perturbers of the same mass. These globular clusters could be detected in radio lens systems with VLBI imaging.

In this paper, we estimate the number density of globular clusters near the Einstein radius of typical early-type galaxies. Using a catalogue of globular clusters in the Virgo cluster (Peng et al. 2008; Jordán et al. 2009), we estimate the strong lensing distortions induced by globular clusters and compare them to the distortions induced by dark matter haloes of the same mass.

The paper is organized as follows. We provide a brief description of the globular cluster catalogue in Section 2. In Section 3, we calculate the number density of globular clusters in the Einstein ring region. In Section 4, we calculate the differences in the lensing effects of globular clusters and dark matter haloes. We summarize our conclusions in Section 5.

2 THE GLOBULAR CLUSTER CATALOGUE

To investigate the distortions induced by globular clusters in strong lensing systems, we first estimate the total number of globular clusters expected in the lens galaxy using the catalogue of globular clusters around galaxies in the Virgo cluster compiled by Peng et al. (2008) and Jordán et al. (2009).

Fig. 1 shows that the total number of globular clusters in this catalogue increases as a function of galaxy stellar mass. A typical lens galaxy in the Sloan Lens ACS (SLACS) sample (Bolton et al. 2008) has a stellar mass of a few 10^{11} $M_\odot$. According to Fig. 1, these galaxies possess more than 5000 globular clusters each. The total number of globular clusters increases as $M^{1.45}$, where M is the stellar mass of the globular cluster. The number of globular clusters is known to be proportional to stellar mass, and may in fact

be linear with total galaxy halo mass (Blakeslee, Tonry & Metzger 1997; Peng et al. 2008; Hudson, Harris & Harris 2014).

3 THE NUMBER DENSITY OF GLOBULAR CLUSTERS

3.1 Projected number density profile

The projected number density of globular clusters as a function of projected radius, R, is well described by a Sérsic (Sérsic 1968) profile:

$$\Sigma(R) = \Sigma_{\rm e} \exp\left[-b_n\left(\left(\frac{R}{R_{\rm e}}\right)^{1/n} - 1\right)\right], \quad (1)$$

where

$$b_n = 2n - \frac{1}{3},$$

with three model parameters $\Sigma_{\rm e}$, $R_{\rm e}$, and n. In this paper, we use the best-fitting model parameters for globular clusters in individual Virgo galaxies derived by Lim et al. (in preparation).

3.2 Mass function

We assume that in the Einstein ring region, only structures whose mass exceeds a certain threshold, $M_{\rm th}$, can be detected. Here, the mass of a globular cluster, $M_{\rm GC}$, is defined as the total mass within its tidal truncation radius as defined by a King model (see equation 12). Hereafter, the mass of a globular cluster will be denoted as $M_{\rm GC}$.

If the globular cluster mass function (GCMF) is independent of distance from the centre of the galaxy, then the surface number density of globular clusters within the projected Einstein radius, $R_{\rm Ein}$, more massive than $M_{\rm th}$ can be written as

$$\Sigma'(>M_{\rm th}, R_{\rm Ein}) = \Sigma(R_{\rm Ein}) \int_{M_{\rm th}}^{M_{\rm max}} \frac{{\rm d}n}{{\rm d}M}(M){\rm d}M, \quad (2)$$

where we set the upper bound, $M_{\rm max}$, to be 10^9 $M_\odot$ and dn/dM is the normalized GCMF, which may be inferred from the globular cluster luminosity function (GCLF) by assuming a (constant) mass-to-light ratio, Υ. We choose the widely used Gaussian GCLFs described by Jordán et al. (2007):

$$\frac{{\rm d}N}{{\rm d}m} = \frac{1}{\sqrt{2\pi}} \exp\left[-\frac{(m-\mu_m)^2}{2\sigma_m^2}\right], \quad (3)$$

where m is the absolute magnitude of a globular cluster, μ_m is the mean globular cluster magnitude, $\mu_m = <m>$, and the dispersion $\sigma_m = <(m-\mu_m)^2>^{1/2}$. The GCMF may be written as

$$\frac{{\rm d}N}{{\rm d}M} = \frac{1}{\ln(10)M} \frac{1}{\sqrt{2\pi}\sigma_M} \exp\left[-\frac{(\log M - \langle \log M\rangle)}{2\sigma_M^2}\right], \quad (4)$$

where the mass and magnitude of a globular cluster are related by

$$m = C - 2.5\log M, \quad (5)$$

and we have

$$\sigma_M = \frac{\sigma_m}{2.5} \quad (6)$$

and

$$\langle \log M\rangle = \int (C - 0.4m)\frac{1}{\sqrt{2\pi}} \exp\left[-\frac{(m-\mu_m)^2}{2\sigma_m^2}\right] {\rm d}m = C - 0.4\mu_m; \quad (7)$$

Table 1. Galaxy stellar mass and NGC number in the Virgo Cluster Catalogue (VCC).

Name	Stellar mass (10^{11} $M_\odot$)
VCC 1226/NGC 4472	5.32 ± 1.10
VCC 1316/NGC 4486	3.02 ± 0.79
VCC 1978/NGC 4649	3.39 ± 0.50
VCC 881/NGC 4406	2.90 ± 0.60
VCC 798/NGC 4382	1.87 ± 0.44
VCC 763/NGC 4374	2.36 ± 0.61

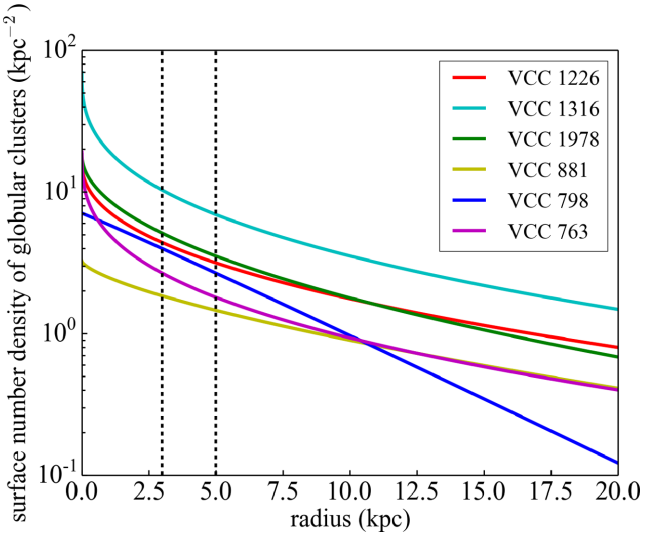

Figure 2. Globular cluster number density profiles of six massive galaxies in the Virgo cluster. The region between the two dashed vertical lines is the range of Einstein radii of typical SLACS lenses.

the constant, C, is related to $\Upsilon = M/L$ through

$$C = 0.4m_\odot + \log\Upsilon, \quad (8)$$

where $m_\odot$ is the absolute magnitude of the Sun.

3.3 Estimate for six massive galaxies in the Virgo cluster

Combining the mass function and number density profile, we can estimate the number of globular clusters in a given mass range projected onto a specific annulus. We estimate the project number density of globular clusters in six massive galaxies in the globular cluster catalogue of the Virgo cluster. The stellar masses of these galaxies are comparable to those of the lens galaxies in the SLACS sample. We list the mass of these six galaxies in Table 1.

We use the values of μ_m and Υ_m derived by Jordán et al. (2007) to calculate the GCLF of galaxies in the Virgo cluster in the z-band. Jordán et al. (2007) showed that Υ is nearly constant with a value of around 1.5 in this band, so we fix $\Upsilon = 1.5$ throughout this paper.

The surface number density profiles of globular clusters in these six galaxies are shown in Fig. 2. With the exception of VCC 798, all other five galaxies have globular cluster surface density profiles of similar form.

We calculate the number density of globular clusters in the annulus between 3 and 5 kpc from the galaxy centre, which is about the Einstein radius of a typical lens in the SLACS survey. The lenses in this survey have a mean velocity dispersion of 275 km s^{-1} and a mean redshift of $z = 0.2$. The results are listed in Table 2.

Table 2. Model predictions for the surface number density of globular clusters around the Einstein rings of six massive early-type galaxies in the Virgo cluster, in units of arcsec^{-2}.

Name	$>10^5$ M$_\odot$	$>10^6$ M$_\odot$	$>10^7$ M$_\odot$
VCC 1226/NGC 4472	29.34 ± 8.62	4.00 ± 1.29	0.0298 ± 0.0169
VCC 1316/NGC 4486	69.79 ± 12.85	8.94 ± 1.79	0.0431 ± 0.0155
VCC 1978/NGC 4649	33.37 ± 14.88	4.45 ± 2.06	0.0316 ± 0.0202
VCC 881/NGC 4406	13.73 ± 2.39	1.78 ± 0.45	0.0085 ± 0.0064
VCC 798/NGC 4382	27.04 ± 8.92	3.12 ± 1.17	0.0112 ± 0.0090
VCC 763/NGC 4374	19.00 ± 12.90	2.26 ± 1.57	0.0062 ± 0.0057

Using ΛCDM N-body simulations, Xu et al. (2015) derived the surface number density of subhaloes in a ΛCDM universe. For subhaloes of mass larger than 10^6 $M_{\rm sub}$ (where the mass refers to the mass assigned by the SUBFIND algorithm that corresponds approximately to the mass within the tidal radius), they found a surface number density of about 1.5 arcsec^{-2} in the strong lensing region of a halo of $10^{13}h^{-1}$ M$_\odot$. As mentioned in the Introduction, in a recent paper, Li et al. (2017) showed that the number density of line-of-sight haloes with effective NFW mass, $M_{\rm eff} > 10^6$ M$_\odot$, is about 5 arcsec^{-2}.

From Table 2, the number density of globular clusters more massive than 10^6 M$_\odot$ is about 1.5–9 arcsec^{-2}, which is comparable to the number density of dark matter perturbers. Since the mass profile of globular clusters is much more concentrated than that of the dark matter haloes (and subhaloes), VLBI observations of radio-selected lenses reaching milli-arcsecond resolution may be strongly affected by the presence of globular clusters. In the rest of this paper, we will show that globular clusters can generate much stronger lensing signals than dark matter haloes of $M_{\rm NFW} = M_{\rm GC}$; they are therefore distinguishable from haloes.

4 THE LENSING EFFECT OF GLOBULAR CLUSTERS

Dark matter haloes and globular clusters have very different density profiles and thus generate different lensing signals. In this section, we compare the distortions induced on the strong lensing images by these different perturbers.

We first assume that the main lens lies at $z_{\rm l} = 0.2$ and we model its density profile with a singular isothermal sphere (SIS) of velocity dispersion, $\sigma_v = 275$ km s^{-1}. A globular cluster or a dark matter halo (subhalo) is then placed at the Einstein radius. A source galaxy whose surface brightness profile is taken to be a Gaussian with dispersion, $\sigma_{\rm source} = 0.02$ arcsec, is assumed to be located at redshift $z_{\rm s} = 0.7$. Using a ray-tracing code, we generate a lensed image on a plane of 8000 × 8000 pixels, each of size 0.7 milli-arcseconds.

Here we consider two types of dark matter perturbers: the subhaloes residing in the dark matter halo of the lens galaxy, and the dark matter haloes along the line of sight.

We assume the line-of-sight haloes have a density profile given by the NFW formula (Navarro, Frenk & White 1996, 1997):

$$\rho(x) = \frac{\rho_{\rm s}}{x(1+x)^2}, \tag{9}$$

where $x = r/r_{\rm s}$ and $r_{\rm s}$ is the scale parameter. The concentration parameter, c, is defined as

$$r_{\rm s} = r_{200}/c, \tag{10}$$

where r_{200} is the radius within which the average interior density equals 200 times the critical density. Hereafter, we use 'NFW' to denote this type of perturber and its mass is defined as the mass enclosed within r_{200}, $M_{\rm NFW}$.

For the subhalo, we additionally include a truncation radius, $r_{\rm t}$, to the NFW model, where

$$r_{\rm t} = R\left(\frac{m}{3M(R)}\right)^{1/3}, \tag{11}$$

where m is the mass of the subhalo, R is the distance between the dark halo and the centre of the host galaxy, and $M(R)$ is the mass of the host galaxy enclosed within R. Hereafter, this type of perturber is denoted as 'sNFW' and the mass of an sNFW subhalo refers to the mass enclosed within the truncation radius, $M_{\rm t}$.

The density profile of the globular cluster is represented with a King model (King 1966). Its density, $\rho(r)$, can be obtained by solving the following equations:

$$\frac{d^2W}{{\rm d}R^2} + \frac{2}{R}\frac{{\rm d}W}{{\rm d}R} = -9\frac{\rho}{\rho_0} \tag{12a}$$

$$\rho = \frac{9}{\rho_0}\exp\left[W - W_0\right]\int_0^W \eta^{-3/2}{\rm e}^{-W}{\rm d}\eta \tag{12b}$$

$$R = r/r_0 \tag{12c}$$

$$\lim_{R\to 0}\frac{2}{R}\frac{{\rm d}W}{{\rm d}R} = -6, \tag{12d}$$

where r_0 is a scale parameter and W_0 and equation (12d) are the initial conditions for equation (12a). The King model has three parameters: W_0, ρ_0, and $M_{\rm GC}$, the mass of the globular cluster. $M_{\rm GC}$ is obtained by integrating a King profile out to its tidal truncation radius, where W reaches zero.

In Fig. 3, we compare the surface density profile of the globular cluster NGC 5139 with the profile of an NFW halo of the same mass. It is clear that the globular cluster distribution is much more concentrated than the NFW halo. The radius of the globular cluster is 72 pc, while the radius of the much more extended dark halo is $r_{200} \sim 2000$ pc.

To compare the strong lensing effects among different perturbers, we generate the perturbed lensing images using globular clusters and fit the images with NFW (sNFW) profiles. To create input data, we use King model parameters derived by McLaughlin & van der Marel (2005) to generate the density profiles of the globular clusters. Here we choose five globular clusters NGC 5139, NGC 6441, NGC 6388, NGC 2808, and NGC 6273, whose mass and profile parameters are shown in Table 3. Fitting results for globular clusters are listed in Table 4.

In Fig. 4, we illustrate the distortions induced on a lensed image by NGC 5139 and by dark haloes of comparable mass. Each panel shows a section of an Einstein ring near the projected position of the perturber. The presence of the perturber distorts the image around it.

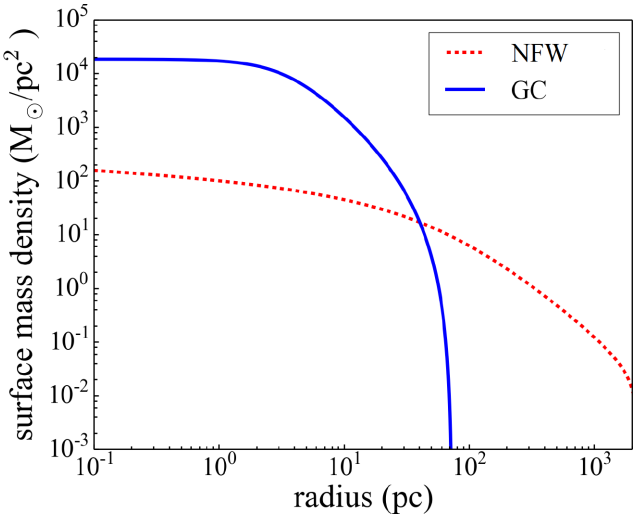

Figure 3. The surface density profile of globular cluster NGC 5139 (solid line) and an NFW dark halo (dotted line) of the same mass. The units of length are parsecs and the units of surface mass density are $M_\odot$ pc^{-2}.

Table 3. King parameters of five globular clusters derived by McLaughlin & van der Marel (2005).

Name	M_{GC} (10^6 $M_\odot$)	ρ_0 (10^4 $M_\odot$ pc^{-3})	W_0
NGC 5139	2.34	0.27	6.2
NGC 6441	1.45	44.67	7.7
NGC 6388	1.05	60.26	7.6
NGC 2808	0.85	8.51	7.1
NGC 6273	0.69	1.86	7.0

Table 4. Fit results. The unit of mass is 10^6 $M_\odot$. For sNFW haloes, we extrapolate their density profile to find r_{200} and calculate the concentration c. We also list the corresponding concentration, c^*, derived from the concentration mass relation given by Neto et al. (2007).

Name	Best-fitting NFW			Best-fitting sNFW		
	M_{NFW}	c	c^*	M_t	c	c^*
NGC 5139	4.44	139300	25.1	2.70	6397	24.6
NGC 6441	2.71	120700	26.5	2.08	27873	25.8
NGC 6388	1.94	105200	27.4	1.52	25088	26.6
NGC 2808	1.57	95840	28.1	1.21	20038	27.2
NGC 6273	1.26	87065	28.8	0.94	12956	27.9

For each type of perturber, we also calculate the average deflection angle with respect to the case of no perturber as follows:

$$d\alpha = \frac{1}{N}\sum_{i}^{N} ||\Delta\alpha^i_{sub} - \Delta\alpha^i_{back}||, \quad (13)$$

where N is the total number of pixels covering an area of 200 pc × 200 pc (total 6400 pixels) centred on the perturber on the lens plane. α^i_{sub} and α^i_{back} are deflection angles for the cases with and without a perturber, respectively. For the globular cluster, we see from Fig. 4 that the induced distortion changes the surface brightness around its position by about 2 per cent; the corresponding $d\alpha$ is 0.998×10^{-3} arcsec.

For a NFW perturber of the same mass, assuming the concentration–mass relation given by Neto et al. (2007), the value of $d\alpha$ is 0.097×10^{-3} arcsec, which is only about 10 per cent of the previous value, resulting in an invisible distortion in the upper right-hand panel of Fig. 4.

The lower two panels of Fig. 4 show the distortions induced by the best-fitting NFW haloes and sNFW haloes to the imaging data, respectively. In both cases, the best-fitting values of r_s are much smaller than is predicted by N-body simulations. The sNFW model, for which $d\alpha = 1.052 \times 10^{-3}$ arcsec, fits the data better than the NFW model for which $d\alpha = 0.866 \times 10^{-3}$ arcsec. For the NFW halo case, although the best-fitting model gives a variation in brightness comparable to that caused by the globular cluster, the differences in the images are still visible by eye.

In Fig. 5, we display the relation between the mass of all five globular clusters and the corresponding best-fitting mass of NFW and sNFW dark haloes. According to Fig. 5, for NFW haloes, the best-fitting mass is about 1.9 times of the corresponding globular clusters, while for sNFW haloes, the best-fitting mass is about 1.25 times of corresponding globular clusters.

Note that the perturbation strength of a line-of-sight NFW halo varies as a function of its redshift. In this work, we fix the redshift of the NFW halo to be the redshift of the lens galaxy. Thus, the best-fitting mass of the line-of-sight NFW halo should be regarded as an 'effective mass'. We refer the reader to Li et al. (2017) and Despali et al. (2017) for a detailed discussion of the relation between effective mass and the true mass of line-of-sight perturbers.

Therefore, if an observation is sensitive enough to detect dark matter perturbers above a certain (effective) mass threshold limit, it should also be able to detect globular clusters of a similar mass. However, our results show that the difference between globular clusters and dark matter perturbers can be readily established from the data: as shown in Table 4, using an NFW (or sNFW) profile to fit a lensed image perturbed by a globular cluster would result in a best-fitting concentration parameter that is hundreds to thousands of times larger than the value predicted by N-body simulations.

Note that, in the ray-tracing test of this work, we do not include observational details such as the point spread function (PSF), source complexity, or noise variation across the image. In reality, however, the systematics induced by these observational effects may couple with the choice of mass model. In a recent paper, Despali et al. (2017) investigated the effects of the PSF on the inferred perturber parameters using *HST* mock datasets and found that the best-fitting values are not biased in this more realistic situation.

To examine the robustness of our conclusions, we repeat the calculation for NGC 5139 assuming different lensing configurations. As shown in Fig. 6, we vary the shape of the lensing galaxy by setting its ellipticity to 0.78, a typical value for SLACS lenses (Koopmans et al. 2006). To investigate possible effects due to external shear, following equation (16) in Despali et al. (2017), we add an external shear of strength $\Gamma = 0.1$. We change the relative positions of lens and source to generate asymmetrical lensing arcs. We locate the perturbers at three different positions on the Einstein arcs, which are marked with white circles in Fig. 6. With the same external shear and elliptical shape for the lens, we also change the redshift of the source to 1.0 and 1.5. Furthermore, to examine the possible effects from the structure of the background source, in the same lens plane configuration as position '1' in Fig. 6, we repeat the ray-tracing test by changing the profile of the source from a Gaussian to elliptical Sersic profile with $R_e = 0.02$ arcsec, axis-ratio $q_{source} = 0.80$, and Sersic index $n = 2$, 3, 4. In Table 5, we list best-fitting parameters

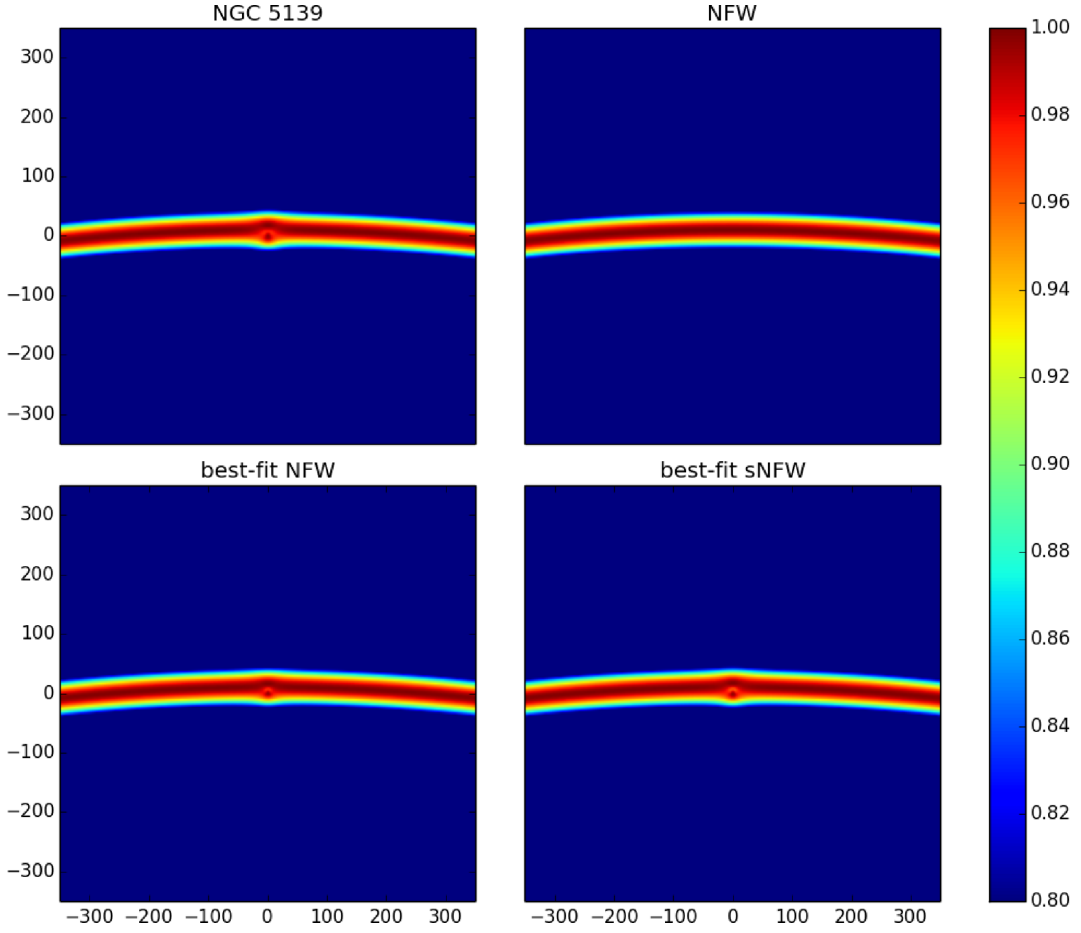

Figure 4. Image of a section of an Einstein ring. The upper left-hand panel illustrates the lensing effect of a globular cluster of mass $10^{6.37}$ $M_{\odot}$, while the upper right-hand panel illustrates the lensing effect of an NFW halo of the same mass. The lower panels show the result of attempting to fit the distortion in the upper left-hand panel assuming, incorrectly, that it is due to an NFW and sNFW dark halo. The best-fitting NFW halo has mass of 4.44×10^6 $M_{\odot}$ and concentration, $c = 10^{5.14}$. The best-fitting sNFW halo has mass of 2.70×10^6 $M_{\odot}$ and concentration, $c = 10^{3.81}$. The axes, showing the physical size in the lens plane, are in units of parsecs.

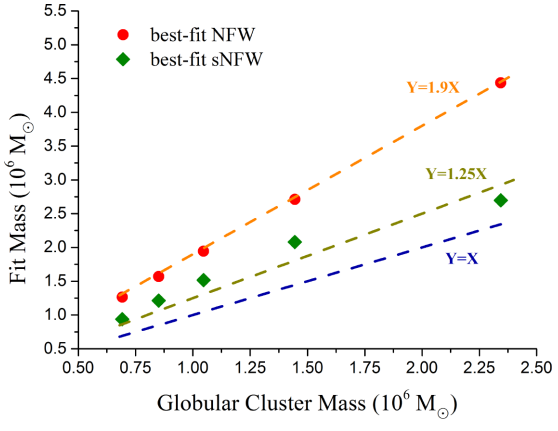

Figure 5. Mass relation between globular clusters and two types of dark matter perturbers. Note that the mass of an NFW and sNFW halo refers to $M_{\rm NFW}$ and $M_{\rm t}$, respectively.

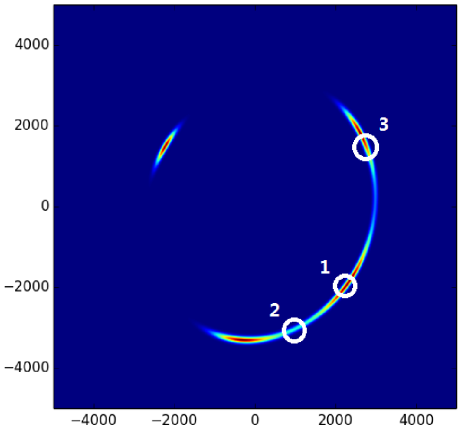

Figure 6. Positions of perturbers in the lensed image. To generate asymmetrical arcs, we chose the lens galaxy to be elliptical and changed the relative positions of the lens and source. Perturbers were placed at centres of the white circles. The axes, showing relative positions in the lens plane, are in units of physical parsecs.

Table 5. The effect of different lensing configurations. Lens type O is the original configuration. Lens type I, II, and III correspond to positions 1, 2, and 3 in Fig. 6, respectively. Types IV and V correspond to the cases where the redshift of the background source is set to 1.0 and 1.5, respectively. Types VI, VII, and VIII are the cases when elliptical Sersic sources with Sersic index $n = 2$, 3, 4, respectively, are assumed. The column 'Difference in mass' is the average difference in mass relative to Lens type O. Here, c^* is the concentration derived from the concentration–mass relation given by Neto et al. (2007) for a halo of the same mass. The units of mass are 10^6 $M_\odot$.

Lens type	Best-fitting NFW			Best-fitting sNFW			Difference in mass
	M_{NFW}	c	c^*	M_t	c	c^*	
O	4.44	139300	25.1	2.70	6397	24.6	N/A
I	4.21	206461	25.2	2.47	4422	24.7	6.85%
II	4.12	511784	25.3	2.37	2927	24.7	9.71%
III	4.32	263587	25.1	2.56	5591	24.8	3.94%
IV	4.38	147504	25.1	2.69	7151	24.7	0.86%
V	3.68	397370	25.6	2.29	2961	24.9	16.15%
VI	4.44	25078	25.1	2.63	2295	24.3	1.30%
VII	2.65	17222	26.5	2.46	3563	24.7	24.60%
VIII	2.77	26897	26.4	2.61	9070	24.8	20.47%

for both NFW and sNFW dark haloes in different lensing configurations for comparison with the previous best-fitting values. As shown in the table, for some of the more complex cases, the difference in mass can be as large as ∼25 per cent, which suggests that there could be residual effects on the best-fitting masses from more realistic lensing configurations. However, in all cases, the best-fitting values of c are still much larger than those predicted for haloes or subhaloes in the simulations.

5 DISCUSSION AND SUMMARY

Small distortions of images of Einstein rings or giant arcs offer the exciting prospect of detecting dark matter haloes or subhaloes too small to have made a visible galaxy. Since a fundamental property of the CDM model of cosmogony, which distinguishes it from other possibilities such as WDM, is the existence of a very large number of such small haloes, detecting them could discriminate between different kinds of dark matter particles, and even rule out the cold dark matter model altogether.

A possible source of contamination of the signal are globular clusters, which can also distort a strong lensed image. These distortions are detectable with milli-arcsecond resolution imaging. In this paper, we have calculated the lensing effect of globular clusters and compared it to the lensing effect of intervening dark matter haloes.

We selected six early-type galaxies in the Virgo cluster of stellar mass $\sim 10^{11}$ $M_\odot$, similar to the mass of strong lens galaxies in the SLAC survey. The number density of globular clusters of mass $\sim 10^6$ $M_\odot$ is between 1.5 and 9 arcsec^{-2}, which is comparable to the number of dark matter perturbers, when both subhaloes and line-of-sight haloes in the same mass range are counted. These globular clusters are not massive enough to be detected through their lensing effects with images taken by *HST* at the typical lens redshift, but the resolution required can be potentially obtained with VLBI-like observations.

We used a ray-tracing method to compare the distortions of the image of an Einstein ring or giant arc induced by a globular cluster and by an NFW (sNFW) halo. We find that the globular cluster produces a much stronger lensing signal than an NFW (sNFW) halo of the same mass, because the density profile of a globular cluster is much more centrally concentrated than that of a dark matter halo.

Imaging at milli-arcsecond resolution can therefore distinguish a globular cluster from a dark matter halo. If an NFW (or sNFW) is used to model the distortion caused by a globular cluster, a poor fit is obtained and the inferred concentration parameter is orders of magnitude higher than the concentration of a real NFW (sNFW) of the same mass. We conclude that globular clusters will not compromise efforts to measure the abundance of low mass dark matter haloes and subhaloes, but their detection would be a byproduct of efforts to constrain the identity of the dark matter from the strong lensing test.

ACKNOWLEDGEMENTS

We acknowledge National Key Program for Science and Technology Research and Development (2017YFB0203300), NSFC grant (Nos. 11773032,118513). QH acknowledges Science and Technology Innovation Training Program of CAS. RL acknowledges support from Newton award, Nebula Talent Program of NAOC, National Key Program for Science and Technology Research and Development (2017YFB0203300) and NSFC grants (Nos 11425312,11503032,11573031 and 118513). EWP and SL acknowledge support from the National Natural Science Foundation of China under grant No. 11573002. This work was supported in part by STFC Consolidated Grant ST/L00075X/1 to Durham and by ERC Advanced Investigator grant, COSMIWAY. This work used the DiRAC Data Centric system at Durham University, operated by the Institute for Computational Cosmology on behalf of the STFC DiRAC HPC Facility (www.dirac.ac.uk). This equipment was funded by BIS National E-infrastructure capital grant ST/K00042X/1, STFC capital grants ST/H008519/1 and ST/K00087X/1, STFC DiRAC Operations grant ST/K003267/1, and Durham University. DiRAC is part of the National E-Infrastructure.

REFERENCES

Benson A. J., Lacey C. G., Baugh C. M., Cole S., Frenk C. S., 2002, MNRAS, 333, 156
Blakeslee J. P., Tonry J. L., Metzger M. R., 1997, AJ, 114, 482
Bolton A. S., Burles S., Koopmans L. V. E., Treu T., Gavazzi R., Moustakas L. A., Wayth R., Schlegel D. J., 2008, ApJ, 682, 964
Bose S., Hellwing W. A., Frenk C. S., Jenkins A., Lovell M. R., Helly J. C., Li B., 2016, MNRAS, 455, 318

Boyarsky A., Ruchayskiy O., Shaposhnikov M., 2009, Annu. Rev. Nucl. Part. Sci., 59, 191
Boyarsky A., Ruchayskiy O., Iakubovskyi D., Franse J., 2014, Phys. Rev. Lett., 113, 251301
Bulbul E., Markevitch M., Foster A., Smith R. K., Loewenstein M., Randall S. W., 2014, ApJ, 789, 13
Bullock J. S., Kravtsov A. V., Weinberg D. H., 2000, ApJ, 539, 517
D'Souza R., Rix H.-W., 2013, MNRAS, 429, 1887
Despali G., Vegetti S., White S. D. M., Giocoli C., van den Bosch F. C., 2018, MNRAS, 475, 5424
Diemand J., Kuhlen M., Madau P., 2007, ApJ, 667, 859
Frenk C. S., White S. D. M., 2012, Ann. Phys., Lpz., 524, 507
Garrison-Kimmel S. et al., 2017, MNRAS, 471, 1709
Green A. M., Hofmann S., Schwarz D. J., 2005, J. Cosmol. Astropart. Phys., 8, 003
Hezaveh Y. D. et al., 2016, ApJ, 823, 37
Hudson M. J., Harris G. L., Harris W. E., 2014, ApJ, 787, L5
Jordán A. et al., 2007, ApJS, 171, 101
Jordán A. et al., 2009, ApJS, 180, 54
Kennedy R., Frenk C., Cole S., Benson A., 2014, MNRAS, 442, 2487
King I. R., 1966, AJ, 71, 64
Koopmans L. V. E., 2005, MNRAS, 363, 1136
Koopmans L. V. E., Treu T., Bolton A. S., Burles S., Moustakas L. A., 2006, ApJ, 649, 599
Li R., Frenk C. S., Cole S., Gao L., Bose S., Hellwing W. A., 2016, MNRAS, 460, 363
Li R., Frenk C. S., Cole S., Wang Q., Gao L., 2017, MNRAS, 468, 1426
Lovell M. R. et al., 2016, MNRAS, 461, 60
Macciò A. V., Moore B., Stadel J., Diemand J., 2006, MNRAS, 366, 1529
McKean J. et al., 2015, Proc. Sci., Strong Gravitational Lensing with the SKA. Sissa, Trieste, PoS#84
McLaughlin D. E., van der Marel R. P., 2005, ApJS, 161, 304
Navarro J. F., Frenk C. S., White S. D. M., 1996, ApJ, 462, 563
Navarro J. F., Frenk C. S., White S. D. M., 1997, ApJ, 490, 493
Neto A. F. et al., 2007, MNRAS, 381, 1450
Okamoto T., Frenk C. S., 2009, MNRAS, 399, L174
Peng E. W. et al., 2008, ApJ, 681, 197
Sawala T. et al., 2016, MNRAS, 456, 85
Sawala T., Pihajoki P., Johansson P. H., Frenk C. S., Navarro J. F., Oman K. A., White S. D. M., 2017, MNRAS, 467, 4383
Sérsic J. L., 1968, Atlas de galaxias australes. Observatorio Astronomico. Cordoba, Argentina
Somerville R. S., 2002, ApJ, 572, L23
Springel V. et al., 2008, MNRAS, 391, 1685
Vegetti S., Koopmans L. V. E., 2009a, MNRAS, 392, 945
Vegetti S., Koopmans L. V. E., 2009b, MNRAS, 400, 1583
Vegetti S., Koopmans L. V. E., Bolton A., Treu T., Gavazzi R., 2010, MNRAS, 408, 1969
Vegetti S., Lagattuta D. J., McKean J. P., Auger M. W., Fassnacht C. D., Koopmans L. V. E., 2012, Nature, 481, 341
Wetzel A. R., Hopkins P. F., Kim J.-h., Faucher-Giguère C.-A., Kereš D., Quataert E., 2016, ApJ, 827, L23
Xu D., Sluse D., Gao L., Wang J., Frenk C., Mao S., Schneider P., Springel V., 2015, MNRAS, 447, 3189

This paper has been typeset from a TEX/LATEX file prepared by the author.